Ocean Climate Change: Comparison of Acoustic Tomography, Satellite Altimetry, and Modeling

The ATOC Consortium

Comparisons of gyre-scale acoustic and direct thermal measurements of heat content in the Pacific Ocean, satellite altimeter measurements of sea surface height, and results from a general circulation model show that only about half of the seasonal and year-to-year changes in sea level are attributable to thermal expansion. Interpreting climate change signals from fluctuations in sea level is therefore complicated. The annual cycle of heat flux is 150 ± 25 watts per square meter (peak-to-peak, corresponding to a 0.2°C vertically averaged temperature cycle); an interannual change of similar magnitude is also detected. Meteorological estimates of surface heat flux, if accurate, require a large seasonal cycle in the advective heat flux.

Changes in oceanic heat storage are a major expected element of future climate shifts. Coupled atmosphere-ocean models are used for understanding the present climate and predicting future states. Testing the ocean component of the coupled models by direct observations is very difficult, however, because climate-scale variability is masked by an intense 100-km spatial-scale variability (the so-called mesoscale) as well as higher frequency internal waves.

Two recently developed observational methods, satellite altimetry and acoustic tomography, are especially suitable for detecting climate-scale changes because they provide large-scale averages. Altimetry depends on the travel time of radio waves reflected at the sea surface. Tomography relies on the travel time of sound waves through the (electromagnetically opaque) ocean interior. The high horizontal resolution of altimetry complements the vertical resolution of acoustic tomography (1). Here we demonstrate that the combined data can extract changes in ocean heat storage on the scale of an ocean basin, the northeast Pacific. Fifteen months of acoustic data from the Acoustic Thermometry of Ocean Climate (ATOC) project in combination with altimeter data from the TOPEX/POSEIDON mission (2) were compared with an oceanic general circulation model and then used to constrain the model.

Physical Setting

We use sea level change (itself of intrinsic interest) as a convenient measure for comparing the different ATOC observations. Sea level change can be inferred from the acoustic measurements (under certain assumptions) for comparison with the direct altimetry measurements, but it is not possible uniquely to do the opposite—to infer heat content from the altimetry measurements for comparison with the "direct" (neglecting salinity) acoustic measurements.

Sea level fluctuations have many causes (3). Daily tides are associated with a divergence in horizontal volume flux with no attendant significant change in density. Direct atmospheric heating and cooling of the water column and exchanges of fresh water are associated with expansion and contraction on time scales from days to millennia. Local changes in temperature and salinity, and hence of density, are also associated with lateral shifts due to ocean currents. Changes with no immediate density signature, as with the tides, are "barotropic" and are not directly relevant to inferences about stored heat; otherwise, changes are "baroclinic." For example, the observed secular rise in sea level (4) is a combination of the melting of glaciers (barotropic) and thermal expansion. Determining the relative contributions of barotropic and baroclinic processes on the myriad time scales of climate change is complex.

Theoretical studies provide some clues as to the relative importance of barotropic and baroclinic fluctuations. A recent model study (5) suggested that wind-driven changes in ocean circulation are largely baroclinic in the tropics, but barotropic at higher latitudes. Observations with sparse current meter moorings in the North Pacific (6) show that on a time scale of 100 days the relative contribution of barotropic processes varied between 10 and 70%, depending on the location. Here we examine the evidence on time scales from months to years.

Observations and Model

Acoustic component. Ocean acoustic tomography (7) has the ability to sample and average the large-scale oceanic thermal structure, synoptically, along several sections and at regular intervals. In late October 1995, the ATOC program deployed an acoustic source at a depth of 939 m on Pioneer Seamount, 100 km west of San Francisco, California (8). Transmissions began in December 1995, and the transmitted signals have been received on U.S. Navy Sound Surveillance System (SOSUS) and other arrays. The arrays consisted of those mounted on the sea floor (for example, k, l, n, and o in Fig. 1) and two 40-hydrophone vertical line arrays (v1 and

The ATOC Consortium: A. B. Baggeroer, T. G. Birdsall, C. Clark, J. A. Colosi, B. D. Cornuelle, D. Costa, B. D. Dushaw, M. Dzieciuch, A. M. G. Forbes, C. Hill, B. M. Howe, J. Marshall, D. Menemenlis, J. A. Mercer, K. Metzger, W. Munk, R. C. Spindel, D. Stammer, P. F. Worcester, and C. Wunsch.* A. B. Baggeroer is in the Department of Ocean Engineering, Massachusetts Institute of Technology (MIT), Cambridge, MA 02139, USA. T. G. Birdsall and K. Metzger are in the Department of Electrical Engineering and Computer Sciences, University of Michigan, Ann Arbor, MI 48109, USA. C. Clark is in the Laboratory of Ornithology, Cornell University, Ithaca, NY 14853, USA. J. A. Colosi is in the Department of Applied Ocean Physics and Engineering, Woods Hole Oceanographic Institution, Woods Hole, MA 02543, USA. B. D. Cornuelle, M. Dzieciuch, W. Munk, and P. F. Worcester are at Scripps Institution of Oceanography, University of California, San Diego, La Jolla, CA 92093, USA. D. Costa is in the Biology Department, University of California, Santa Cruz, CA 95064, USA. B. D. Dushaw, B. M. Howe, J. A. Mercer, and R. C. Spindel are at the Applied Physics Laboratory, University of Washington, Seattle, WA 98105, USA. A. M. G. Forbes is at the Division of Oceanography, CSIRO, Hobart, Tasmania 7001, Australia. C. Hill, J. Marshall, D. Menemenlis, D. Stammer, and C. Wunsch are in the Department of Earth, Atmospheric and Planetary Sciences, MIT, Cambridge, MA 02139, USA.

*To whom correspondence should be addressed.

Table 1. Annual harmonic amplitude (in centimeters) and, in parentheses, phase (in days) of range-averaged sea level anomaly (η) along the acoustic sections.

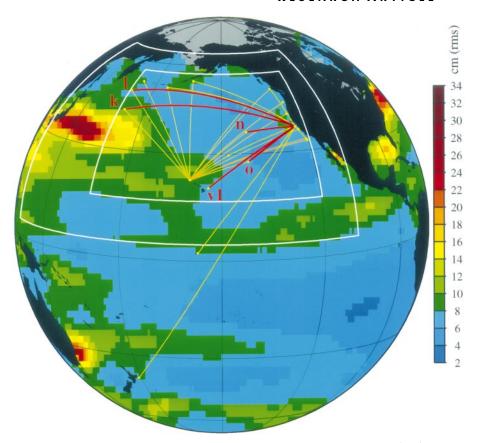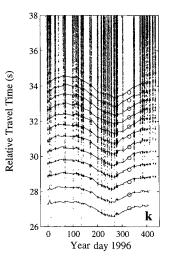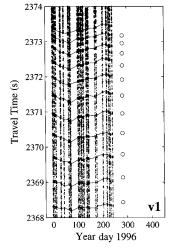| Component	Acoustic section				
	l	k	n	o	v1
η_{clim}	2.5 (273)	2.9 (291)	2.1 (284)	2.0 (277)	2.5 (272)
η_{acoust}	2.9 (255)	2.5 (257)	2.0 (270)	2.3 (302)	0.8 (59)
η_{XBT}					2.7 (304)
η_{GCM}	2.5 (262)	3.3 (266)	1.7 (287)	1.0 (270)	0.7 (278)
η_{altim}	4.0 (271)	4.9 (276)	4.0 (281)	3.6 (275)	3.6 (282)

Fig. 1. The ATOC acoustic array is superimposed on a map of the root-mean-square (rms) sea level anomaly from 4 years (January 1993 to December 1996) of TOPEX/POSEIDON altimetric measurements. Red lines indicate the sections used in the present study and are referenced by letter labels. Yellow lines show additional sections along which the acoustic propagation has been observed, but for which the data were not used here. Data assimilation was carried out in the region bounded by the outer white rectangle, and heat content estimates were obtained inside the inner white rectangle. Much, but not all, of the elevation anomalies represent seasonal thermal changes within the ocean, with the acoustic data providing a stable spatial average that is otherwise difficult to obtain. The ATOC region, being on the eastern side of the ocean, shows comparatively weak variability. Nevertheless, it is evident that the different acoustic sections will, during any 10-day period, have potentially very different anomalies.

missions are spaced 4 hours apart during transmission periods. A total of 772 transmissions in 43 groups were made between December 1995 and March 1997 (*10*). A recognizable one-to-one correspondence exists between the observed and predicted ray arrivals (Fig. 2). This result and other work (*11*) show that at these ranges, ray arrivals are resolvable, identifiable, and stable. Ray arrivals were tracked and then used to infer range-averaged profiles of sound speed and temperature along each section (*12*). Despite the presence of mesoscale eddies and internal waves, the arrival times vary smoothly through the months as a result of the spatial integration.

The vertical resolving power of the acoustic data is determined by the ray structure. For sections k and l, all identified rays are steep and surface reflecting and have lower turning depths between 2000 and 3500 m. For sections n and o, identifiable rays begin as surface reflecting near the source and change to near-surface refracting as they approach the receivers. Section v1 has both surface-reflecting and purely refracting rays.

The travel times for section k (Fig. 2), and with one exception, all other sections, decreased in the summer and increased in the winter, consistent with the expected seasonal heating and cooling of the surface layer. For section v1, the situation was different: maximum heat content was recorded in March 1996. From a comparison of sections o and v1 (Fig. 3), we infer that the winter surface layer cooling near the source, where the two sections overlap, was more than offset by a subsurface warming near receiver v1, where the rays do not sample the surface layer.

Altimetric component. The TOPEX/POSEIDON altimeter (*13*), in a 10-day repeating orbit, produces precise and accurate measurements of the sea surface topography (Fig. 1). Sea surface topography can be used to determine motions that extend deep into the oceanic interior (*14*), but its structure reflects a complex combination of many different physical processes, barotropic and baroclinic. Other data, such as acoustic or expendable temperature profiler (XBT) data, and theory [including general circulation models (GCMs)] are used to separate the various components by geography and by space-time scales.

Direct temperature measurements. XBT surveys from ships were conducted adjacent to section v1 (Fig. 3). Such surveys provide a direct measure of the heat content of the upper ocean (<800 m). Repetition of the surveys is, however, difficult to arrange. Climatologies (*15*) (multidecadal averages of historical data) are able to provide rough estimates of the mean seasonal cycle of heat and salinity changes.

Modeling component. Ocean GCMs are

v2). Vertical arrays permit the detailed study of the received acoustic signals. The trans-

mission schedule typically consists of 4-day periods, two to four times a month (*9*). Trans-

Fig. 2. Acoustic arrival patterns for receivers k and v1 at approximate ranges of 5000 and 3000 km, respectively. Arrival patterns are presented as "dot plots," where the dot size is proportional to the signal-to-noise ratio. Predicted ray arrivals (open circles) were generated with a climatology (*15*) and then shifted in time to optimize the comparison. Only the early arrivals, corresponding to steep rays, are tracked (solid lines). Rays propagating at shallow angles arrive in quick succession and are more difficult to resolve. Receiver v1, a 40-element vertical line array, permits a cleaner reception than receiver k, which is a horizontal array mounted on the sea floor.

a representation of Newton's laws of motion and thermodynamics for the fluid ocean driven at the sea surface through exchanges with the atmosphere of stress (winds) and buoyancy fluxes (heat and fresh water). We used a GCM constructed for ATOC (*16*) that "predicts" the fields observed by acoustic tomography and altimetry.

Comparison of the Data

Each of the measurement types—acoustic, altimetric, and XBT—can be used to produce an estimate of components of the sea level anomaly, η_{acoust}, η_{altim}, and η_{XBT}, respectively, over all or part of the domain. The available climate estimate, η_{clim}, is restricted to the mean seasonal cycle (*15*). Another estimate, η_{GCM}, comes from the GCM.

The altimetric and GCM records roughly track the climatological annual cycle, albeit with different amplitudes (Table 1) and with obvious evidence of both higher frequency and interannual variability. Acoustic results also track η_{clim} for all sections except v1, but they do not exhibit the short period fluctuations of η_{altim} and η_{GCM}. Differences between η_{altim} and η_{acoust} (2.4 cm rms) result from salt and barotropic contributions to η present in η_{altim}, as well as from uncertainties in the altimetric and acoustic estimates.

The amplitude of η_{acoust} at the annual period is, on average, half that of η_{altim}. Similarly η_{XBT}, which is consistent with the acoustic data during the overlapping period, has an rms difference from η_{altim} of 2.9 cm, larger than the likely errors in the altimetric (~1 cm rms) and XBT (~0.2 cm rms for the 800-m thermal contribution) measurements (*17*). A small number of salinity measurements along section v1 suggest a considerable (~2 cm rms) salt contribution to η on seasonal to interannual time scales, especially in the transition zone between the low-salinity waters of the California Current and saltier subtropical waters offshore.

Short-period fluctuations in η_{altim} and η_{GCM} are primarily caused by wind-forced barotropic Rossby waves. These waves are not sensed either by the acoustic (*18*) or temperature measurements. A study (*19*) comparing XBT and altimetric data over a period of 4 years along a trans-Pacific section concluded that about 80% of the variance of η_{altim} and η_{XBT} was coherent at wavelengths of 500 to 3000 km, which could be interpreted as implying a barotropic variance contribution of about 20%.

Insufficient information exists to separate fully the salt, thermal, and mass contributions to the low-frequency sea level anomaly from data alone (*6*), but a partial estimate can be obtained from the GCM prediction. Of the total GCM sea level variability in the ATOC region, 28% lies in the barotropic mode at periods exceeding a few months, and this serves as our a priori estimate of low-frequency mass contributions to η_{altim}. All estimates of sea level variability are consistent if in this area 1/3 to 1/2 of the low-frequency variance is contributed by processes not reflecting heat content changes.

Model-Data Combinations

Because the observations and the model produce independent estimates of the oceanic fluctuations with distinctly different expected errors, we can attempt a statistical best estimate of the oceanic state through their formal combination (*20*). Let $\mathbf{x}_{ocean}(t)$ represent the true oceanic state vector defined as a set of physical quantities (typically velocity, temperature, salinity, and surface pressure) on a three-dimensional grid that, along with initial and boundary conditions, provides sufficient information to calculate the oceanic state one time step, Δt, in the future:

$$\mathbf{x}_{ocean}(t + \Delta t) = L[\mathbf{x}_{ocean}(t), \mathbf{u}(t), \mathbf{q}(t)] \quad (1)$$

Operator L represents the GCM (a lengthy computer code), vector $\mathbf{u}(t)$ comprises known elements of initial and boundary conditions, and vector $\mathbf{q}(t)$ comprises unknown elements of initial and boundary conditions, indeterminate model parameters (for example, mixing coefficients), and other errors in the physics of the model. We assumed that the second moment matrix, $\mathbf{Q}(t) = \text{cov}[\mathbf{q}(t)]$, is at least
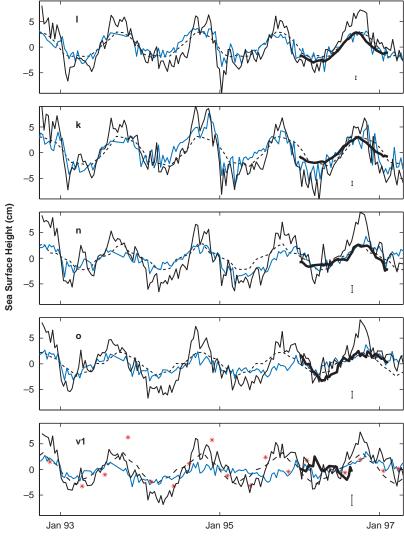
Fig. 3. The range-averaged sea level anomaly along the acoustic sections inferred by several independent methods: (i) thick black lines indicate the ATOC acoustic measurements converted to equivalent sea surface height for comparison with the altimeter data, (ii) thin black lines are from the TOPEX/POSEIDON altimeter data, (iii) dashed lines represent the climatological thermal anomaly converted to sea surface height, (iv) blue lines are the GCM estimates, and (v) the asterisks along section v1 are the XBT data. Uncertainties are indicated for the acoustic estimates: the possible errors are largest along section v1 because the upper ocean variability is unresolved due to a lack of surface-reflecting rays near the receiver.
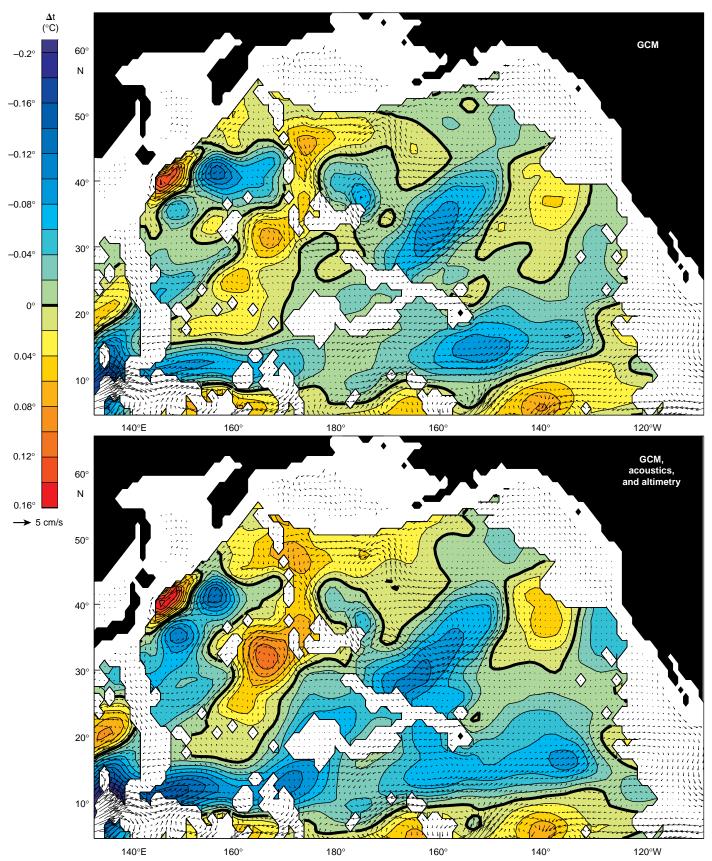
Fig. 4. The upper panel depicts the GCM-predicted temperature change, averaged over the top 4000 m, from January 1996 to January 1997. The arrows indicate the corresponding change in velocity at 610 m. White regions indicate depths less than 4000 m in the GCM. The lower panel depicts the same quantities, but after combination of the GCM with the acoustic and altimetric data. The data require significant changes in what the GCM alone computes.

approximately known. All GCMs set $\mathbf{q}(t) = 0$, producing an estimate, $\mathbf{x}_{GCM}(t)$, of the oceanic state, which differs from $\mathbf{x}_{ocean}(t)$.

Observations, be they acoustic or altimetric, can be viewed as measuring the departure of the GCM prediction from the real ocean. We define $\mathbf{y}(t)$ to be measurements of the model-data difference:

$$\mathbf{y}(t) = \mathbf{E}(t)\mathbf{x}_{error}(t) + \mathbf{n}(t) \qquad (2)$$

where $\mathbf{x}_{error} = \mathbf{x}_{GCM} - \mathbf{x}_{ocean}$, $\mathbf{E}(t)$ is a known "observation" matrix specifying the relation between model elements and the observations, and the measurement error, $\mathbf{n}(t)$, is assumed to have zero mean with known covariance $\mathbf{R}(t)$.

Those elements of the model that are uncertain (including initial and boundary conditions and inadequate physics) lead to errors in calculating the oceanic state that are detectable in the observations, thus permitting correction of the model elements. Conversely, for those elements of the oceanic state that are poorly observed or not observed at all, the model will provide a realistic estimate, and the combination of the model and the data produces a better estimate than either could alone.

We use a scheme (21) based on linear estimation theory and on a coarse resolution representation of $\mathbf{x}_{error}(t)$ consisting of four vertical temperature modes, 8° samples in the horizontal, and monthly samples in time. Smaller unresolved scales as well as salt and barotropic effects become part of the observational noise, $\mathbf{n}(t)$, and their dynamical consequences are accounted for in the control term, $\mathbf{q}(t)$; that is, $\mathbf{R}(t)$ and $\mathbf{Q}(t)$ are now taken to represent the covariances of the deficiencies in the reduced-state linear model as well as those in the GCM. A
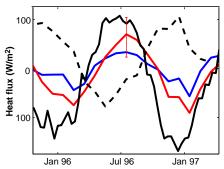
priori covariances for the various problem unknowns are based on the comparisons already described (22).

Circulation and Heat Budget

The above model-data combination produces a best estimate of the heat content, barotropic, and salinity changes. Comparison of the January 1996 to January 1997 temperature change from the GCM alone (Fig. 4, top panel) to that from the GCM-altimeter-acoustic combination (Fig. 4, bottom panel) shows that the GCM alone approximately simulates interannual variations in heat content changes, for example, the broad diagonal bands of warmer and colder water crossing the basin from southwest to northeast. But, in general, the GCM underestimates the magnitude of these changes, which can be as large as 0.2°C averaged over the top 4000 m. Changes in the current fields reflect large (up to 5 cm/s at 610-m depth) fluctuations in the tropical Pacific velocity field (Fig. 4). Substantial interannual changes are also observed at midlatitudes, away from the relatively quiet northeastern Pacific. About 50% of the sea level variance on time scales of months to years and spatial scales exceeding about 1500 km is contributed by the change in heat content. Altimetric-acoustic differences apparently result from a barotropic mass redistribution, with variable salt anomalies a contributing, but smaller, factor.

The top-to-bottom heat content anomaly in the region spanned by the ATOC array, 168° to 240°E, 16° to 56°N, converted to equivalent sea surface heat flux (Fig. 5) shows that the GCM underestimates the strength of the seasonal cycle as compared with the combined GCM-altimeter-acoustic combination. This deficiency, present in almost all state-of-the-art ocean models, results from missing information on the mixed-layer physics and errors in the surface boundary conditions. The heat budget (23, 24) of this region can be further elucidated by comparing these heat content estimates to the surface heat flux from meteorological analyses. Assuming that the two estimates are perfect, their difference would be proportional to the advective component of heat flux entering the region. If atmospheric estimates of direct heat transfer are reliable to $\pm$ 30 W/m² (25), the difference indicates a surprisingly large (3) seasonal cycle in the advective components (180 W/m² peak-to-peak surface equivalent). The result is consistent in magnitude and phase with previous tomographic estimates (24) of 50 to 150 W/m² advected into a triangle centered at 160°W and 35°N. Advective heat transports here appear to be an important component in the regional heat budget, accounting for about half the seasonal variation in oceanic heat storage.

Climate models attempting to describe

and predict the coupled ocean-atmosphere heat budget are now quantitatively testable on scales exceeding 1000 km at the equivalent accuracies of less than 2 cm rms in sea level. These values place stringent demands on the models for accurate calculation of barotropic and baroclinic components. They require great care in dealing with the exchange of fresh water across the air-sea interface and raise serious questions about the accuracy of conventional meteorological estimates.

References and Notes

1. W. Munk and C. Wunsch, *Philos. Trans. R. Soc. London Ser. A* **307**, 439 (1982).
2. A demonstration of this system (TOPEX/POSEIDON: Ocean TOPography EXperiment/Premier Observatoire Spatial Étude Intensive Dynamique Ocean et Nivosphere) on a much smaller scale in the western Mediterranean, was described [D. Menemenlis, A. T. Webb, C. Wunsch, U. Send, C. Hill, *Nature* **385**, 618 (1996)].
3. J. G. Patullo, W. H. Munk, R. Revelle, E. Strong, *J. Mar. Res.* **14**, 88 (1955); C. Wunsch, *Rev. Geophys.* **10**, 1 (1972); A. E. Gill and P. P. Niiler, *Deep Sea Res.* **20**, 141 (1973).
4. M. F. Meier, *Science* **226**, 1418 (1984); R. S. Nerem *et al.*, *Geophys. Res. Lett.* **24**, 1331 (1997).
5. I. Fukumori, R. Raghunath, L.-L. Fu, *J. Geophys. Res.* **103**, 5493 (1998).
6. Current meter data indicate that the surface kinetic energy in this region is about 5% barotropic [C. Wunsch, *J. Phys. Oceanogr.* **27**, 1770 (1997)]. Direct quantitative estimates of the barotropic contribution to η (the sea level anomaly) cannot, however, be made easily from these data because of lack of knowledge about the wave number characteristics of the barotropic mode.
7. W. Munk, P. F. Worcester, C. Wunsch, *Ocean Acoustic Tomography* (Cambridge Univ. Press, New York, 1995).
8. B. M. Howe, *Technical Memo 3-96* (Applied Physics Laboratory, University of Washington, 1996); ATOC Instrumentation Group, *Oceans '95* **3**, 1483 (1995).
9. The transmission schedule is determined by the sampling requirements of the associated ATOC Marine Mammal Research Project. The biological elements of ATOC have been the source of controversy (A. S. Frankel and C. W. Clark, *Can. J. Zool.*, in press; see also http://atoc.ucsd.edu).
10. The transmitted signal is phase modulated and encoded by using a linear maximal shift register sequence containing 1023 digits. The transmission parameters of the signal are as follows: center frequency 75 Hz, bandwidth 37.5 Hz (quality factor, $Q = 2$), power 260 W (195 dB relative to 1 μPa at 1 m), sequence period 27.28 s, digit length 26.667 ms, and total duration 44 periods or 1200.32 s. A coded signal is necessary to overcome transducer peak power limitations; although the noise level of the source blends with oceanic background levels within a few hundred kilometers, the signal processing makes it possible to hear the source at great distances, >10,000 km, as if all the transmitted energy was contained in a single 26.667-ms digit pulse. Beam forming is used to determine the arrival angle and further increase the signal-to-noise ratio. The ability to do phase-coherent beam forming at these ranges came as a pleasant surprise.
11. P. F. Worcester *et al.*, *J. Acoust. Soc. Am.*, in preparation.
12. Although it is the low-frequency components of the travel time signals that are of most importance here, the high-frequency components are used to study the internal wave field [J. A. Colosi, S. M. Flatté, C. Bracher, *ibid.* **96**, 452 (1994)] and the tides [B. D. Dushaw et al., *Prog. Oceanogr.* **40**, 337 (1997)]. The acoustic travel time fluctuations at tidal frequencies compare very favorably with those predicted by the latest tide models.
13. L.-L. Fu *et al.*, *J. Geophys. Res.* **99**, 24369 (1994); C.

Fig. 5. Heat content change inside the region spanned by the acoustic array (inner box in Fig. 1) from the GCM (blue line) and the GCM-altimeter-acoustic estimate (red line and associated error bar), converted to an equivalent sea surface heat flux per unit area for comparison with estimates from the NCEP (black line). The difference between NCEP and the GCM-altimeter-acoustic estimates (dashed line) indicates the advective component at the lateral boundaries of the region or errors in either or both of the atmospheric or oceanic fields.

Wunsch and D. Stammer, *Annu. Rev. Earth Planet. Sci.* **26**, 219 (1998).

14. The elevation changes represent the gradients in the oceanic surface pressure field, and there is a corresponding fluid flow that is the general circulation. A 1-cm surface elevation change over 100 km of lateral distance at midlatitudes corresponds to about 1 cm/s of velocity or about 7×10^9 kg/s of fluid movement if the corresponding pressure gradient extends to the sea floor [C. Wunsch and D. Stammer, *J. Geophys. Res.* **100**, 24895 (1995); D. Stammer, *ibid*. **102**, 20987 (1997)].

15. S. Levitus, R. Burgett, T. P. Boyer, *NOAA Atlas NESDIS 3* (Government Printing Office, Washington, DC, 1994); S. Levitus and T. P. Boyer, *NOAA Atlas NESDIS 4* (Government Printing Office, Washington, DC, 1994).

16. The GCM is that of J. Marshall, A. Adcroft, C. Hill, L. Perelman, and C. Heisey [*J. Geophys. Res.* **102**, 5753 (1997)]. It was initialized from a climatological hydrography (*15*) and integrated in a global configuration with realistic topography, 1° horizontal grid spacing, and 20 vertical levels. Starting in 1985, the GCM was driven with surface fluxes from the U.S. National Centers for Environmental Prediction (NCEP) analyses. Surface wind stress is specified from estimates at 12-hour intervals. Surface buoyancy forcing (heat flux and evaporation minus precipitation) comes from 24-hour interval estimates. In addition to the buoyancy terms, the surface layer temperature and salinity are forced toward monthly NCEP sea surface temperature analyses and seasonal Levitus climatology, respectively, to compensate for inadequacies in the model physics and forcing fields. Forcing strengths (time scales) are from B. Barnier, L. Siefridt, and P. Marchesiello [*J. Mar. Sys.* **6**, 363 (1995)]. By the start of the TOPEX/POSEIDON observations in late 1992, the model has reached a near-statistical equilibrium (some residual model drift, particularly in the abyssal ocean, does persist, but it should be immaterial for the time scales being examined here).

17. A discussion of the altimetric error budget appears in (*13*). At wavelengths on the order of 1000 km and larger, the altimetric error (including atmospheric, orbit, and tidal contributions) amounts to 4.9 cm rms along each individual track. The uncertainty is reduced to 1 cm rms by averaging over many tracks. The XBT error, converted to a steric height anomaly for the top 800 m of water, is of the order of 1.3 cm per profile, and again it is much reduced by the averaging of sequential profiles.

18. The contribution of temperature to one-way travel time perturbations is one to two orders of magnitude larger than that of salt or current (*7*). Ocean currents have been measured by obtaining the difference in the travel times of acoustic signals traveling in opposite directions; B. D. Dushaw, P. F. Worcester, B. D. Cornuelle, and B. M. Howe [*J. Geophys. Res.* **99**, 3263 (1994)] found megameter-scale currents of only about 1 cm/s in the central North Pacific.

19. Results are from 16 colocated trans-Pacific XBT surveys over a 4-year period concurrent with the TOPEX/POSEIDON altimetric mission. Sparse salinity data were also collected and used to determine the salt contribution to sea level anomaly (J. Gilson, D. Roemmich, B. Cornuelle, L.-L. Fu, *J. Geophys. Res.*, in press).

20. C. Wunsch, *The Ocean Circulation Inverse Problem* (Cambridge Univ. Press, New York, 1996); R. Daley, *Atmospheric Data Analysis* (Cambridge Univ. Press, New York, 1991).

21. I. Fukumori, *J. Geophys. Res.* **100**, 25027 (1995); D. Stammer and C. Wunsch, *ibid*. **101**, 18409 (1996); D. Menemenlis and C. Wunsch, *J. Atmos. Oceanic Technol*. **14**, 1420 (1997).

22. The estimation results and their uncertainty are functions of the prior covariance matrices for the system and measurement errors, $Q(t)$ and $R(t)$, respectively. Here we use diagonal, time-independent, prior covariance matrices for Q and for the altimetric R. Q has variance consistent with the variance of GCM-hydrographic differences in the North Pacific. R has variance 9 cm^2, which includes altimeter noise (1 cm^2) and barotropic-salinity model errors (8 cm^2). For acoustic data, a full covariance R is derived on the basis of the seasonal climatology (*15*), and on the particular transmission characteristics along each section. D. Menemenlis and M. Chechelnitsky (*Mon. Weather Rev.*, in press) discuss model and data errors in more detail.

23. W. B. White and C.-K. Tai, *J. Geophys. Res.* **100**, 24943 (1995); J. Hsiung, R. E. Newell, T. Houghtby, *Nature* **325**, 518 (1987).

24. B. D. Dushaw, P. F. Worcester, B. D. Cornuelle, B. M. Howe, *J. Phys. Oceanogr*. **23**, 2650 (1993).

25. The meteorological analyses are not accompanied by an error bar for the estimated air-sea heat flux, and this absence is a major obstacle to further quantitative progress in many climate problems. A recent estimate [J. R. Moisan and P. Niiler, *ibid*. **28**, 401 (1998)] confirms that bulk formula errors are probably in the range of 20 to 40 W/m^2; these errors may well be systematic.

26. Acoustic thermometry owes its development to continuing support by the Office of Naval Research. This work was also supported by the Strategic Environmental Research and Development Program through the Defense Advanced Research Projects Agency, the Department of Energy, and NASA and by grants of computer time from project SCOUT at the MIT Laboratory for Computer Science.

6 March 1998; accepted 28 July 1998

Science

Ocean Climate Change: Comparison of Acoustic Tomography, Satellite Altimetry, and Modeling
The ATOC Consortium

ARTICLE TOOLS	http://science.sciencemag.org/content/281/5381/1327
RELATED CONTENT	file:/contentpending:yes
REFERENCES	This article cites 22 articles, 2 of which you can access for free http://science.sciencemag.org/content/281/5381/1327#BIBL
PERMISSIONS	http://www.sciencemag.org/help/reprints-and-permissions